

A Novel Chemical Reduction Route towards the Synthesis of Crystalline Nickel Nanoflowers from a Mixed Source

Xiaomin Ni,^[a] Qingbiao Zhao,^[a] Huagui Zheng,^{*[a]} Beibei Li,^[a] Jimei Song,^[a]
Dongen Zhang,^[a] and Xiaojun Zhang^[a]

Keywords: Nickel / Nanostructures / Chemical reduction / Crystal growth

A novel chemical reduction route was designed for the synthesis of nickel nanocrystals with distinct flowery shapes by using a mixture of two complexes of $\text{Ni}(\text{N}_2\text{H}_4)_3^{2+}$ and $\text{Ni}(\text{dmg})_2$ (nickel dimethylglyoximate) as the nickel source. Formation of these flowers, comprising spherical centers and swordlike petals, was related to the varying stability and structural properties of the two precursors as well as the reaction conditions. Investigations of the time-dependent shape-evolution process indicated that spherical particles were

formed first as flower centers, and then swordlike petals grew radially from the particle surfaces. A rational mechanism of formation was proposed on the basis of a range of contrasting experiments. Compared with bulk nickel, these nanoflowers exhibited an enhanced coercivity (H_c) and a decreased saturation magnetization (M_s); this fact is attributed to their peculiar morphology.

(© Wiley-VCH Verlag GmbH & Co. KGaA, 69451 Weinheim, Germany, 2005)

Introduction

For many years, control of the morphology of nanomaterials has been of great interest for their shape-dependent properties and potential applications in nanoelectronics, photonics, magnetics, catalysis, and so forth.^[1] Exploration of various shape-controlling synthetic methods and studies on their unusual properties will inevitably drive the progress in nanotechnology. Templates such as macroporous membranes, carbon nanotubes, aluminum anode oxides (AAO), block copolymers, microemulsions, polymers, and complexing agents are often utilized during synthesis to control the shape of nanomaterials.^[2] Among these templates, utilizing coordination complexes as precursors has attracted particular attention for its simplicity and convenience. A range of novel-shaped nanocrystals have been fabricated by this method, for example Cu_2O nanowires, cubic FeS_2 crystallites, and several different shaped ZnO nanostructures including hollow spheres, ringlike nanosheets standing on spindlelike rods, nanoparticles nanoribbons, flowerlike cupped-end microrod bundles, branched spindles, and prismatic whiskers.^[3] In this technique, the morphology of the target product was closely associated with the structure and shape of the complex precursors. Upon removal of the ligand molecules in a rational and controllable manner, inorganic nanomaterials with the desired size and shape could be synthesized.^[3c]

In addition to the effect of templates, modification of the reaction steps also has great influence on the crystal configuration. Generally, the formation processes of crystals include nucleation and growth, which is practically a continuous process. However, in the two-step, seed-mediated synthesis technique, the nucleation and growth are purposely separated for adjusting the crystal morphology. In the first step, the seed nanocrystals, whose characteristic symmetry and structure are critical for directing the final crystal shape, are synthesized and added to the synthetic system. Then, precursors to the desired structures are chemically reduced in the presence of capping molecules and seed nanocrystals that serve as nucleation sites.^[4] Following this methodology, a series of different shaped nanocrystals were fabricated. For example, uniform Au and Ag nanorods, dumbbell-shaped Au–Ag core-shell nanocrystals were all created from the seed-mediated growth in solution.^[5a–5c] Oriented arrays of ZnO nanorods were produced from citrate solution in the presence of nanosized ZnO seeds.^[5d] Likewise, using Ag nanoparticles as seeds, a peculiar netlike Ag skeleton could be synthesized by reduction of silver ions with Raney nickel.^[5e] These results indicate this synthetic approach has great potential for the anisotropic growth of inorganic nanocrystals, but the interface issues between the seed and growing materials have not been well resolved, and further research is required for their general applicability and extension to the synthesis of complex nanostructures.^[4b]

Nanosized particles of nickel have diverse applications in the fields of catalysis, magnet recording, medical diagnosis, and conduction.^[6] In the past decade, nickel nanocrystals with the following shapes have been fabricated: nanotubes,

[a] Department of Chemistry, University of Science and Technology of China, Hefei, Anhui, 230026, People's Republic of China
Fax: +86-551-3601600
E-mail: hgzheng@ustc.edu.cn

hollow spheres, nanobelts, nanorods, nanoprisms, and hexagonal flakes. However, the creation of nickel nanoflowers has seldom been reported.^[7] In this paper, we have designed a new reaction route which combines coordination control with the step modulation technique and yields nickel nanocrystals with a novel flower shape. This strategy involves the monitoring of crystal nucleation and growth through chemical reactions. In contrast to previous methods using a single-source precursor, two complexes, $\text{Ni}(\text{N}_2\text{H}_4)_3^{2+}$ and $\text{Ni}(\text{dmg})_2$, comprise the nickel source. The reaction process involves two steps: firstly, $\text{Ni}(\text{N}_2\text{H}_4)_3^{2+}$ is reduced, and the resulting spherical nanocrystals serve as the flower centers. Then, $\text{Ni}(\text{dmg})_2$ yields swordlike nanocrystals which grow radially on the existing spherical centers as petals. A series of experiments were conducted to investigate the possible formation process.

Results and Discussion

The phase and purity of the as-prepared product was determined by X-ray diffraction (XRD), as shown in Figure 1. All the diffraction peaks could be indexed as face-centered cubic (fcc) nickel (JCPDS 01–1260). No characteristic peaks due to the impurities of nickel oxides or hydroxides were detected, indicating that pure crystalline nickel was fabricated under such conditions.

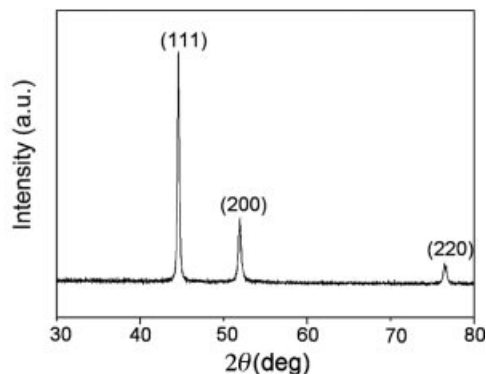


Figure 1. XRD pattern of as-prepared flowerlike nickel crystals.

The morphology of the sample was investigated by field emission scanning electron microscopy (FE-SEM) and transmission electron microscopy (TEM). A low-magnification image, shown in Figure 2a, demonstrates that the product exhibits novel flowerlike shapes. A magnified image of an individual crystallite indicated that the flower comprised dozens of swordlike petals radiating from the center, which can be seen in Figure 2b. The petals with sharp ends and protruding surface ridges have sizes in the range of 30–80 nm in diameter, 20–50 nm in thickness, and 0.5–2.0 μm in length. Sonication for 10 min did not break this nanostructure into discrete particles, indicating that the nanoflowers were actually integrated, and were not only aggregations of spherical and swordlike particles. TEM images of the nanoflowers with petals assembled at the center, agreeing well with the FE-SEM observations, can be seen in Fig-

ure 2c. Besides the flowerlike nanostructures, it was noted that a small fraction of hexagonal flakes (about 1%, as arrowed in Figure 2a) emerged in the final product. Shown in Figure 2d is a TEM image of two overlapping flakes with a side length of about 100 nm. The corresponding selected area electron diffraction (SAED) pattern indicated that they are also due to fcc nickel.

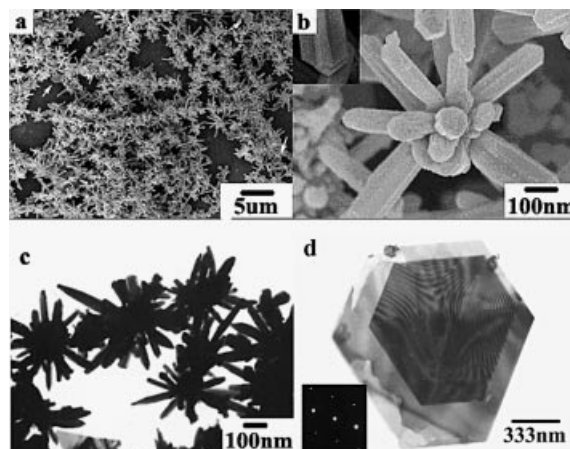


Figure 2. SEM images of as-prepared samples: (a) a low-magnification SEM image; (b) a high-magnification SEM image of an individual flower (the inset is a typical petal); TEM images of the sample: (c) several typical nickel flowers; (d) two overlapping hexagonal flakes of fcc Ni.

More details of the flowerlike structure were investigated by high resolution transmission electron microscopy (HRTEM) and SAED. A typical sharp-ended petal (Figure 3a) with a diameter of about 20 nm was chosen as the object of investigation. The HRTEM image in Figure 3b shows three sets of lattice spacings of ≈ 0.20 , 0.18, and 0.12 nm that are in accordance with the separation between the (111), (200), and (220) planes of fcc Ni, respectively. From the HRTEM image, the growth direction of the petal could be indexed as along $[01\bar{1}]$. The corresponding ED pattern in Figure 3c was recorded with the electron beam along the $[011]$ zone axis, revealing the single crystalline nature of the petal. It was noted that in the SAED pattern additional diffraction spots along the directions of $[111]$ and $[200]$ appeared, which implied the presence of five superlattices in both directions.

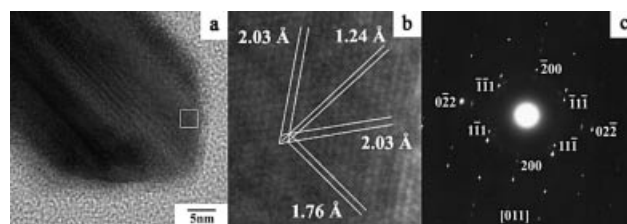


Figure 3. (a) TEM image of the tip of a typical petal. (b) HRTEM image taken from the petal. (c) The corresponding SAED pattern, taken from the $[011]$ zone axis. The additional diffraction spots along $[111]$ and $[200]$ implied the presence of five superlattices of nickel in these two directions.

To probe into the growth process of the nanoflowers, we studied the shape evolution of the product over time by FE-SEM. Figure 4 shows the images of three samples hydrothermally treated for 3 h, 7 h, and 11 h, respectively (Figure 4a, b, and c). It was shown that spherical nickel particles with diameters of about 100 nm emerged as the initial product after the mixture was heated at 120 °C for 3 h. With time, short rods grew out on these spherical particles, and some particles developed into flowery crystals. After 11 h, most of the product had evolved into flower-shaped crystal-lites with swordlike petals.

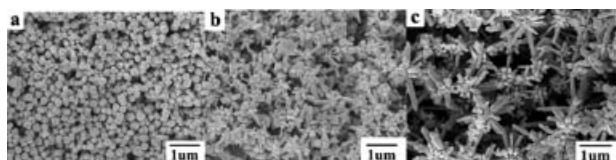
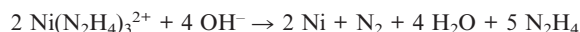


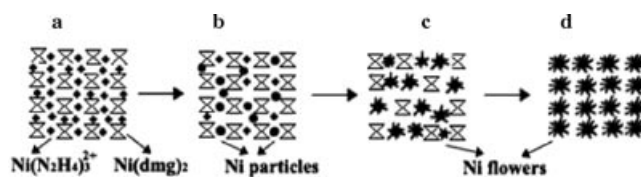
Figure 4. SEM images of the samples obtained at different reaction stages. (a) 3 h, (b) 7 h, (c) 11 h.

On the basis of previous studies of nickel nanocrystals from different complexes and the evolution of nickel flowers described above, the possible mechanism of formation of the nickel nanoflowers was detailed. It is known that Ni^{2+} ions can react with dimethylglyoxime (dmgH) and hydrazine (N_2H_4) in aqueous solution to form the complexes of $\text{Ni}(\text{dmg})_2$ and $\text{Ni}(\text{N}_2\text{H}_4)_3^{2+}$, respectively. In basic solution, the $\text{Ni}(\text{N}_2\text{H}_4)_3^{2+}$ (with an instability constant of 4.5×10^{-8}) can react with OH^- in the following manner:



When the pH of the solution was above 12 and the temperature was higher than 85 °C, the reaction proceeded very fast and produced spherical particles.^[8] Because of its higher stability (with an instability constant of 4×10^{-24}) and special planar square structure, $\text{Ni}(\text{dmg})_2$ reacted with hydrazine at a relatively slow rate and yielded nickel nanocrystals with a hexagonal flakelike shape.^[9,71] In our system, about 60 mol-% Ni^{2+} ions were coordinated by dmgH and the rest yielded $\text{Ni}(\text{N}_2\text{H}_4)_3^{2+}$. These two complexes coexisted in one system and comprised the nickel source. However, because of their different stability and structure, they were reduced at different reaction stages and resulted in differently shaped particles. $\text{Ni}(\text{N}_2\text{H}_4)_3^{2+}$ was reduced first and yielded spherical particles, which were dispersed in the system. As the reaction proceeded, $\text{Ni}(\text{dmg})_2$ was attacked, and the newly formed nickel atoms tended to spontaneously

transfer onto the surfaces of the existing particles which served as seed sites for further growth. Because of the higher stability of $\text{Ni}(\text{dmg})_2$, the reaction rate at this stage slowed down, and the concentration of nickel atoms was not enough for the former spherical particles to grow from the circumference. This would lead to undersaturation around the existing particles, and the continuous addition of nickel atoms to the as-formed particle surface would preferentially occur at the active sites of the circumferential edges which had relatively higher free energies than other sites on the surface. As a result, a flowerlike structure was formed because of the lack of mass transport of nickel atoms to the seed particles for their further growth.^[10] The reduced particles grew around each seed particle until all the $\text{Ni}(\text{dmg})_2$ was reduced, eventually resulting in radially oriented petals on the surfaces. It is worth noting that the growth of nickel nanocrystals from $\text{Ni}(\text{dmg})_2$ proceeded in a different manner relative to that from $\text{Ni}(\text{N}_2\text{H}_4)_3^{2+}$. As a special planar complex, $\text{Ni}(\text{dmg})_2$ imposes obvious confinement on the growth of the resultant particles, orienting them along a certain direction.^[71] Therefore, anisotropic petals with swordlike shapes were produced. A schematic pattern of the formation process is shown in Scheme 1. However, it is interesting that the petals did not grow into hexagonal flakes as before, but mainly into swordlike rods, which may be attributed to the effect of the spherical nanocrystals formed at the initial stage. Since the seed particles greatly affected the shape of the crystals, the nickel nanocrystals grown in the presence of spherical particles may develop into a different shape.^[11] In fact, if the spherical nanoparticles were prepared first and then dispersed into the system with $\text{Ni}(\text{dmg})_2$ and hydrazine, a similar flowerlike nanostructure (as seen in Figure 5c) could also be pro-



Scheme 1. Schematic illustration of the formation process of the nickel nanoflowers. (a) mixture of $\text{Ni}(\text{dmg})_2$ and $\text{Ni}(\text{N}_2\text{H}_4)_3^{2+}$ complexes in the system. (b) spherical nickel nanoparticles were formed which came from the reduction of $\text{Ni}(\text{N}_2\text{H}_4)_3^{2+}$ (c) part of the spherical nickel particles had evolved into small flowers with the reduction of $\text{Ni}(\text{dmg})_2$. (d) nickel nanoflowers emerged as the final product.

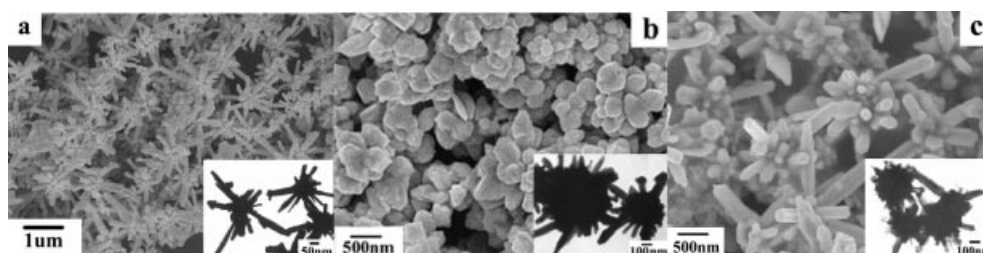


Figure 5. SEM and TEM images of the samples from the system with different molar ratios (ω) of $\text{Ni}(\text{N}_2\text{H}_4)_3^{2+}$ to $\text{Ni}(\text{dmg})_2$ (a) $\omega = 20:80$ (b) $\omega = 80:20$, (c) TEM image of the sample in which the spherical particles were added externally to the system.

duced, which supported the two-step formation process proposed above.

Following the formation of the nickel flowers, it was rationally proposed that the size of the flower centers and petals could be adjusted by changing the molar ratio (ω) of $\text{Ni}(\text{N}_2\text{H}_4)_3^{2+}$ to $\text{Ni}(\text{dmg})_2$, considering their different contribution to the flowerlike structure. This supposition was validated by the FE-SEM images of two samples obtained at different ω values while the other reaction conditions were kept the same. Figure 5a and b shows the images of two samples from the systems with ω values of 20:80 and 80:20, respectively. It is clear that increasing the proportion of $\text{Ni}(\text{dmg})_2$ obviously promoted the size of petals, while a higher proportion of $\text{Ni}(\text{N}_2\text{H}_4)_3^{2+}$ led to flowers with bigger centers.

In all the samples, a small quantity of hexagonal nickel flakes appeared regardless of the reaction time and the ratio of the two Ni sources, as shown in Figure 2, Figure 4, and Figure 5. It was believed that they originated solely from the precursor of $\text{Ni}(\text{dmg})_2$, and not through the two-step process observed above for the flowers. When $\text{Ni}(\text{dmg})_2$ is the only source of nickel, hexagonal flakelike nickel crystals can be produced exclusively. The current system, however, became inhomogeneous because of flocculent $\text{Ni}(\text{dmg})_2$ suspended in the solution, which caused differences in the local concentrations of the reactants. In places where the concentration of hydrazine was relatively high, part of $\text{Ni}(\text{dmg})_2$ would be reduced simultaneously with $\text{Ni}(\text{N}_2\text{H}_4)_3^{2+}$ and directly developed into flakes. Careful observations indicated that small hexagonal flakes appeared even when the mixture was only heated for 3 h (shown in Figure 4a), which well validated our supposition.

The present synthetic route monitored crystal nucleation and growth through two matching chemical reactions in one system. For the two complexes, their different stability resulted in reduction reactions at different stages, and the different structures resulted in particles with different shapes. Cooperation of the two precursors was responsible for the formation of the unique flowerlike nanostructure. Controlled experiments show that, keeping the rest of the conditions the same, substitution of the two complexes with other pairs of Ni sources such as $\text{Ni}(\text{NH}_3)_6^{2+}$ - $\text{Ni}(\text{dmg})_2$, $\text{Ni}(\text{N}_2\text{H}_4)_3^{2+}$ - $\text{Ni}(\text{C}_4\text{H}_2\text{O}_6)^{2-}$ (tartrate), $\text{Ni}(\text{N}_2\text{H}_4)_3^{2+}$ - $\text{Ni}(\text{C}_9\text{NOH}_7)_2$ (nickel 8-hydroxyquinoline), or $\text{Ni}(\text{NH}_3)_6^{2+}$ - $\text{Ni}(\text{en})_3^{2+}$ (ethylenediamine) did not all result in nanoflower formation (as seen in Figure 6). This lack of nanoflower formation is possibly due to a mismatch of the stability or structure of the two starting materials, which did not meet the conditions required for the formation of the flowers. The role of the temperature was also studied, and it was found that the flowers could be reproducibly prepared over an optimized temperature range of 100–150 °C. Temperatures above 150 °C led to spherical particles due to a faster reducing rate, while at temperatures below 100 °C, $\text{Ni}(\text{dmg})_2$ was not completely reduced.

It is known that the magnetic properties of nanomaterials are closely related to the sample size, shape, crystallinity etc. The M - H hysteresis loop of the flowers obtained was

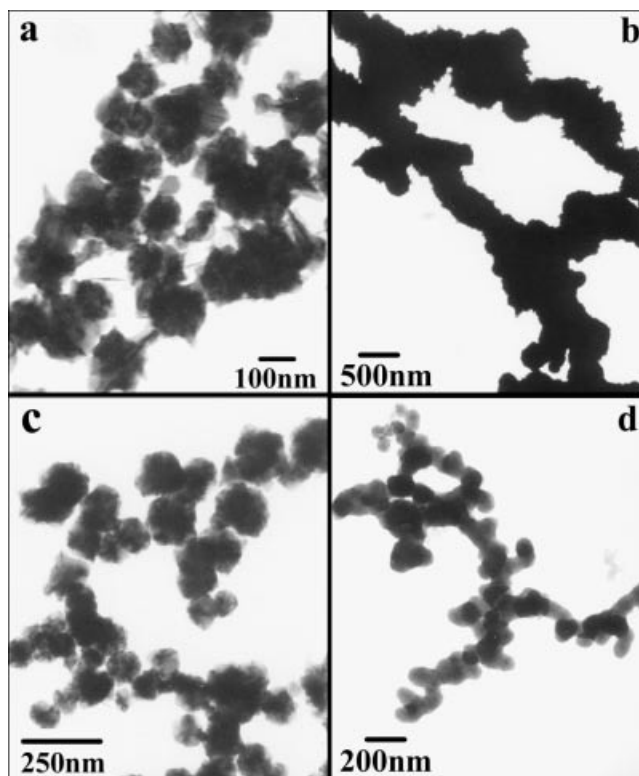


Figure 6. TEM images of the samples prepared from the other mixed nickel sources. (a) $\text{Ni}(\text{NH}_3)_6^{2+}$ - $\text{Ni}(\text{dmg})_2$; (b) $\text{Ni}(\text{N}_2\text{H}_4)_3^{2+}$ - $\text{Ni}(\text{C}_4\text{H}_2\text{O}_6)^{2-}$ (tartrate); (c) $\text{Ni}(\text{N}_2\text{H}_4)_3^{2+}$ - $\text{Ni}(\text{C}_9\text{H}_7\text{NO})_2$ (nickel 8-hydroxyquinoline); (d) $\text{Ni}(\text{NH}_3)_6^{2+}$ - $\text{Ni}(\text{en})_3^{2+}$ (ethylenediamine).

measured at room temperature (Figure 7), showing coercivity (H_c), saturation magnetization (M_s), and remanent magnetization (M_r) values of approximately 173.2 Oe, 30.8 emu g^{-1} , and 9.9 emu g^{-1} , respectively. Compared with that of the bulk nickel (100 Oe, 55 emu g^{-1} , 2.7 emu g^{-1}), the H_c value was much enhanced. As ultrafine ferromagnetic particles often exhibit enhanced coercivity relative to the corresponding bulk material, the small size and shape anisotropy of the flowers may be responsible for the increased H_c value.^[12] However, it was noted that this value was much lower than that of the 1D nanorods (332 Oe) or nanobelts (640 Oe), which was possibly attributed to the special 3D

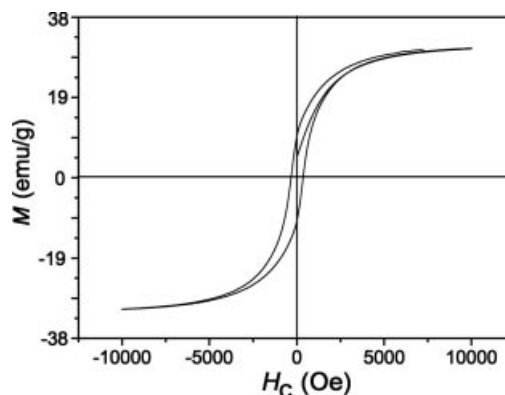


Figure 7. Magnetic hysteresis loop of as-prepared nickel nanoflowers measured at room temperature.

flowerlike structure. Because of the radial orientation of the petals, it was difficult for all of them to be aligned simultaneously along the direction of the external magnetic field compared with the 1D nanomaterials. Therefore, a relatively low H_c value was observed.^[13,7e] As for the decrease in M_s , it might likewise be due to the decrease in particle size accompanied by an increased surface area, together with the magnetic interaction between the petals, which reduced the total magnetic moment at a given field.^[14]

Conclusions

Flower-shaped nickel nanocrystals were successfully prepared by reduction of the mixed complexes of $\text{Ni}(\text{N}_2\text{H}_4)_3^{2+}$ and $\text{Ni}(\text{dmg})_2$ in alkaline solution with hydrazine hydrate. Spherical nickel nanocrystals formed first from $\text{Ni}(\text{N}_2\text{H}_4)_3^{2+}$ and served as the nucleation sites for the growth of the swordlike petals, which originated from the reduction of $\text{Ni}(\text{dmg})_2$. The different stability and structure of the two complexes played an important role in the formation of the distinct nickel nanoflowers. The size of the flower centers and petals could be adjusted by changing the molar ratio of the two complexes. Due to their unique flowery shapes, these crystals exhibited an enhanced coercivity and a decreased M_s value as compared with that of bulk nickel. The present work realized the control of the crystal shape through rationally matching different chemical reactions to adjust the crystal nucleation and growth processes. Such a novel and facile strategy is being further explored for the preparation of other materials under controlled conditions.

Experimental Section

X-ray diffraction (XRD) patterns of the samples were recorded with a Philips X'pert diffractometer with $\text{Cu-K}\alpha$ radiation ($\lambda = 0.15418$ nm). Field emission scanning electron microscopy (FE-SEM) images were recorded with a JEOL JSM-6300F SEM. Transmission electron microscopy (TEM) images were collected with a Hitachi, H-800 electron microscope with an accelerating voltage of 200 kV. High-resolution transmission electron microscopy (HRTEM) images and the selected area electron diffraction (SAED) patterns were recorded with a JEOL-2010 TEM at an acceleration voltage of 200 kV. M-H hysteresis loops were recorded with a vibrating sample magnetometer (BHV-55) at an applied field of 10^4 Oe and a magnetization scale of 2.5 emu on a 0.0352 -g sample sealed in a 6.6×10^{-2} mL vessel.

Nickel chloride ($\text{NiCl}_2 \cdot 6\text{H}_2\text{O}$), dimethylglyoxime (dmgH), sodium hydroxide (NaOH) were all of analytical purity. In a typical experiment, $\text{NiCl}_2 \cdot 6\text{H}_2\text{O}$ (0.166 g) was dissolved in distilled water (25 mL) to give a green transparent solution. Then an ethanol solution (13 mL) containing 1 wt.-% dmgH was added dropwise into the solution. Red flocculates emerged, indicating the formation of $\text{Ni}(\text{dmg})_2$. Subsequently, $\text{N}_2\text{H}_4 \cdot \text{H}_2\text{O}$ (2.0 mL, 80 wt.-%) was added under continuous stirring. The solution pH was adjusted to above 12 using sodium alkali. The mixture was stirred for 30 min and transferred into a Teflon-lined autoclave with a capacity of 50 mL. The autoclave was sealed, heated at 110 °C for 12 h, and then cooled naturally to room temperature. The resulting black powders

were collected and washed, and finally dried in vacuum at 60 °C for 4 h.

- [1] a) A. P. Alivisatos, *Science* **1996**, *271*, 933–937; b) C. B. Murray, D. J. Norris, M. G. Bawendi, *J. Am. Chem. Soc.* **1993**, *115*, 8706–8715; c) K. M. Krishnan, A. P. Alivisatos, *Science* **2001**, *291*, 2115–2117; d) R. Heitz, S. Rodt, A. Schliwa, D. Bimberg, *Phys. Status Solidi B* **2003**, *238*, 273–280; e) R. Narayanan, M. A. El-Sayed, *Nano Lett.* **2004**, *4*, 1343–1348.
- [2] a) J. K. N. Mbindyo, T. E. Mallouk, J. B. Mattzela, I. Kratochvilova, B. Razavi, T. M. Jackson, T. S. Mayer, *J. Am. Chem. Soc.* **2002**, *124*, 4020–4026; b) Y. Zhang, H. Dai, *Appl. Phys. Lett.* **2000**, *77*, 3015–3017; c) D. S. Xue, L. Y. Zhang, A. B. Gui, X. F. Xu, *Appl. Phys. A: Mater. Sci. Process* **2005**, *80*, 439–442; d) D. Zhang, L. Qi, J. Ma, H. Cheng, *Chem. Mater.* **2001**, *13*, 2753–2755; e) X. Zhang, Y. Xie, F. Xu, X. B. Tian, *J. Colloid Interface Sci.* **2004**, *274*, 118–121; f) H. Q. Cao, Z. Xu, H. Sang, D. Sheng, C. Y. Tie, *Adv. Mater.* **2001**, *13*, 121–123; g) Y. Deng, G. Wei, C. Nan, *Chem. Phys. Lett.* **2003**, *368*, 639–643.
- [3] a) Y. Xiong, Z. Li, R. Zhang, Y. Xie, J. Yang, C. Wu, *J. Phys. Chem. B* **2003**, *107*, 3697–3702; b) X. Chen, Z. Wang, J. Wan, J. Liu, Y. Qian, *Inorg. Chem.* **2005**, *44*, 951–954; c) Z. Li, Y. Xie, Y. Xiong, R. Zhang, *New J. Chem.* **2003**, *27*, 1518–1521; d) B. Liu, S. H. Yu, F. Zhang, L. Li, Q. Zhang, L. Ren, K. Jiang, *J. Phys. Chem. B* **2004**, *108*, 4338–4341; e) Z. Gui, J. Liu, Z. Wang, L. Song, Y. Hu, W. Fan, D. Chen, *J. Phys. Chem. B* **2005**, *109*, 1113–1117; f) C. Jiang, W. Zhang, G. Zou, W. Yu, Y. Qian, *J. Phys. Chem. B* **2005**, *109*, 1361–1363; g) H. S. Qian, S. H. Yu, J. Y. Gong, L. B. Luo, L. L. Wen, *Cryst. Growth Des.* **2005**, *5*, 935–939.
- [4] a) Y. W. Jun, S. M. Lee, N. J. Kang, J. Cheon, *J. Am. Chem. Soc.* **2001**, *123*, 5150–5151; b) S. M. Lee, S. N. Cho, J. Cheon, *Adv. Mater.* **2003**, *15*, 441–444.
- [5] a) C. J. Murphy, N. R. Jana, *Adv. Mater.* **2002**, *14*, 80–82; b) C. C. Huang, Z. Yang, H. T. Chang, *Langmuir* **2004**, *20*, 6089–6092; c) Z. R. Tian, J. A. Voigt, J. Liu, B. Mckenzie, M. J. McDermott, M. A. Rodriguez, H. Konishi, H. F. Xu, *Nat. Mater.* **2003**, *2*, 821–826; d) Z. R. Tian, J. A. Voigt, J. Liu, B. Mckenzie, M. J. McDermott, M. A. Rodriguez, H. Konishi, H. F. Xu, *Nat. Mater.* **2003**, *2*, 821–826; e) Y. C. Zhu, M. R. Ji, H. G. Zheng, Y. Li, Z. P. Yang, Y. T. Qian, *Mater. Lett.* **2004**, *58*, 1121–1126.
- [6] a) W. X. Zhang, C. B. Wang, H. L. Lien, *Catal. Today* **1998**, *40*, 387–395; b) V. F. Puentes, K. M. Krishnan, A. P. Alivisatos, *Science* **2001**, *291*, 2115–2117; c) M. P. Pileni, *Adv. Funct. Mater.* **2001**, *11*, 323–336; d) R. Hernandez, S. Polizu, S. Turenne, L. Yahia, *Bio-Med. Mater. Eng* **2002**, *12*, 37–45; e) A. Smogonov, A. Dal Corso, E. Tosatti, *Surf. Sci.* **2002**, *507*, 609–614.
- [7] a) J. Bao, C. Tie, Z. Xu, Q. Zhou, D. Shen, Q. Ma, *Adv. Mater.* **2001**, *13*, 1631–1633; b) J. Bao, Y. Liang, Z. Xu, L. Si, *Adv. Mater.* **2003**, *15*, 1832–1835; c) J. S. Bradley, B. Tesche, W. Buser, M. Maase, M. T. Reetz, *J. Am. Chem. Soc.* **2000**, *122*, 4631–4636; d) N. Cordente, R. M. Espaud, F. Secocq, M. J. Casanove, C. Amiens, B. Chaudret, *Nano Lett.* **2001**, *1*, 565–568; e) Z. Liu, S. Li, Y. Yang, S. Peng, Z. Hu, Y. Qian, *Adv. Mater.* **2003**, *15*, 1946–1948; f) X. Ni, L. Cheng, H. Zheng, D. Zhang, Q. Zhao, J. Song, *Chem. Lett.* **2004**, *33*, 1564–1565.
- [8] a) Y. D. Li, C. W. Li, H. R. Wang, L. Q. Li, Y. T. Qian, *Mater. Chem. Phys.* **1999**, *59*, 88–90; b) G. Schwarzenbach, A. Zobrist, *Helv. Chim. Acta* **1952**, *35*, 129.
- [9] W. Chang, K. Li, *Concise Handbook of Analytic Chemistry*, 1st ed., Science Press **1980**, p. 75.
- [10] a) H. Zhang, D. Yang, X. Ma, Y. Ji, J. Xu, D. Que, *Nanotechnology* **2004**, *15*, 622–626; b) Z. P. Liu, S. Li, Y. Yang, Z. K. Hu, S. Peng, J. B. Liang, Y. T. Qian, *New J. Chem.* **2003**, *27*, 1748–1752.
- [11] A. Gole, C. J. Murphy, *Chem. Mater.* **2004**, *16*, 3633–3640.
- [12] a) J. H. Hwang, V. P. Dravid, M. H. Teng, J. J. Host, B. R. Elliott, D. L. Johnson, T. O. Mason, *J. Mater. Res.* **1997**, *12*,

- 1076–1082; b) D. L. Leslie-Pelecky, R. D. Rieke, *Chem. Mater.* **1996**, *8*, 1770–1783; c) H. O. Cao, Z. Xu, H. Sang, D. Sheng, C. Y. Tie, *Adv. Mater.* **2001**, *13*, 121–123; d) T. M. Whitney, J. S. Jiang, P. C. Searson, C. L. Chien, *Science* **1993**, *261*, 1316–1319.
- [13] X. M. Ni, X. B. Su, Z. P. Yang, H. G. Zheng, *J. Cryst. Growth* **2003**, *252*, 612–617.
- [14] a) D. H. Chen, S. H. Wu, *Chem. Mater.* **2000**, *12*, 1354–1360; b) N. Cordente, C. Amiens, B. Chaudret, M. Respaud, F. Senocq, M. J. Casanove, *J. Appl. Phys.* **2003**, *94*, 6358–6365; c) K. V. P. M. Shaf, A. Gedanken, R. Prozorov, J. Balogh, *Chem. Mater.* **1998**, *10*, 3445–3450.

Received: May 19, 2005

Published Online: October 25, 2005